



**HAL**  
open science

# Monitoring the Degradation of Metal-Organic Framework Drug Nanocarriers by In-situ NMR Spectroscopy

Mai Dang Le Vuong, Mohamed Haouas, Ruxandra Gref, Charlotte Martineau-Corcros

► **To cite this version:**

Mai Dang Le Vuong, Mohamed Haouas, Ruxandra Gref, Charlotte Martineau-Corcros. Monitoring the Degradation of Metal-Organic Framework Drug Nanocarriers by In-situ NMR Spectroscopy. *European Journal of Inorganic Chemistry*, 2024, 10.1002/ejic.202400012 . hal-04567505

**HAL Id: hal-04567505**

**<https://hal.science/hal-04567505v1>**

Submitted on 28 May 2024

**HAL** is a multi-disciplinary open access archive for the deposit and dissemination of scientific research documents, whether they are published or not. The documents may come from teaching and research institutions in France or abroad, or from public or private research centers.

L'archive ouverte pluridisciplinaire **HAL**, est destinée au dépôt et à la diffusion de documents scientifiques de niveau recherche, publiés ou non, émanant des établissements d'enseignement et de recherche français ou étrangers, des laboratoires publics ou privés.



Distributed under a Creative Commons Attribution - NonCommercial - NoDerivatives 4.0 International License

# Monitoring the Degradation of Metal-Organic Framework Drug Nanocarriers by *In-Situ* NMR Spectroscopy

Mai Dang Le Vuong,<sup>[a, b]</sup> Mohamed Haouas,<sup>\*[a]</sup> Ruxandra Gref,<sup>[b]</sup> and Charlotte Martineau-Corcoss<sup>\*[a, c]</sup>

An accurate characterization methodology is indispensable to design nanoparticle-based drug delivery system (DDS) adapted to specific diseases and therapies. However, characterization techniques employed to investigate drug release and nanoparticle degradation require separating the nanoparticles from their suspension media, which can lead to artefacts. Therefore, there is a clear need to implement novel versatile *in-situ* methods. Here, we report the use of *in-situ* NMR spectroscopy to monitor drug delivery processes from MOF nanocarriers, both in solution and in the solid state simultaneously. *In-situ* <sup>1</sup>H NMR investigation of nanoMIL-100(Al) suspension in phosphate medium enabled recording the trimesate ligand loss in the solid

phase and the ligand release in the liquid phase as a function of time. Simultaneously, <sup>27</sup>Al NMR enabled assessing the progressive replacement of carboxylate ligands by phosphates leading to the formation of new aluminum species. Using the same strategy, we also compared the degradation of nanoMIL-100(Al) loaded with two drug analogs, highlighting an effect of metal-ligand complexing strength. Furthermore, our *in-situ* technique is applicable to studying the reaction of paramagnetic nanoMIL-100(Fe) in the liquid phase. This work offers an alternative to *ex-situ* techniques for understanding the degradation mechanism of MOF nanocarriers and could be an asset for other nanoscale DDSs.

## 1. Introduction

Nanoparticles (NPs) are the most prominent nanomaterials in commercial nanotechnology products (78% in 2021).<sup>[1]</sup> In the medicine industry, NP-based drug delivery systems (DDSs) have contributed to the clinical approval of innovative drugs.<sup>[2,3]</sup> Covid vaccine based on NPs and, in another example, Onpatro, consisting in the encapsulation of unstable nucleic acid into a nanocarrier, stabilize these active ingredients and their intracellular delivery into liver cells.<sup>[4]</sup> Along with the engineering of NPs for unmet medical needs, the development of accurate characterization methods is also essential to ensure reproducible batch-to-batch performance of a NP formulation during clinical testing and large-scale production.<sup>[5-7]</sup> The need for *in-situ* techniques for single-particle,<sup>[8]</sup> in-line,<sup>[9]</sup> or *in-situ* characterization,<sup>[10]</sup> is particularly beneficial for NP-based DDSs, as many nanocarrier characterization measurements require proper separation of NP suspensions. For example, determining

drug payload requires quantification of free drug molecules into supernatant and bound drug molecules into precipitated NPs. Common separation techniques such as filtration or (ultra)centrifugation risk disturbing the state and the dynamics of the investigated NP suspension, potentially decreasing the measurement reliability. Therefore, it will be advantageous to study the NP suspension as it is, by reproducing results closer to reality than *ex-situ* techniques to investigate the mechanisms of drug release, nanocarrier degradation, and the interaction of NPs with biological substances.

Several *in-situ* studies monitor drug delivery processes from NPs without separation using fluorescent label-related techniques<sup>[11,12]</sup> or label-free spectroscopy.<sup>[9,13,14]</sup> For instance, Artzi et al. investigated the degradation of polyethyleneglycol (PEG)-dextran hydrogel by following the fluorescence intensity of the polymer PEG conjugated with a fluorescent tag, showing a good correlation between *in vitro* and *in vivo* measurements.<sup>[12]</sup> The limitation of this approach is that one needs to incorporate a fluorescent tag in the specimen and ensure it stays attached in the timeframe of the experiment. There are other *in-situ* studies using label-free techniques, mostly based on spectroscopy.<sup>[9,13,15]</sup> In addition to Raman and IR spectroscopies, NMR spectroscopy has proven valuable for characterizing *in-situ* DDSs, as it can provide both qualitative and quantitative information while being a non-destructive technique. NMR spectroscopy is particularly useful to examine the evolution of molecular structure upon NP formulation, drug loading, drug release, and degradation processes and quantify the proportion of the drug and carrier. Diluted NPs dispersion can be measured by liquid NMR (lqNMR) spectroscopy, while suspensions with high viscosity or high concentration are suitable for solid-state NMR (ssNMR) and high-resolution magic-angle spinning (HR-MAS) NMR.<sup>[16]</sup> Note that in most cases, solid-

[a] M. D. L. Vuong, M. Haouas, C. Martineau-Corcoss  
Institut Lavoisier de Versailles (ILV), Université Paris-Saclay, UVSQ, CNRS,  
Versailles, 78000, France  
E-mail: mohamed.haouas@uvsq.fr

[b] M. D. L. Vuong, R. Gref  
Institut des Sciences Moléculaires d'Orsay (ISMO), Université Paris-Saclay,  
CNRS, Orsay, 91405, France

[c] C. Martineau-Corcoss  
Current Address: CortecNet, 91940 Les Ulis, France  
E-mail: charlotte.martineau@gmail.com

© 2024 The Authors. European Journal of Inorganic Chemistry published by Wiley-VCH GmbH. This is an open access article under the terms of the Creative Commons Attribution Non-Commercial NoDerivs License, which permits use and distribution in any medium, provided the original work is properly cited, the use is non-commercial and no modifications or adaptations are made.

state species cannot be detected by the lqNMR technique. In contrast, liquid species can be recorded in a ssNMR instrument but with compromising spectra quality compared to a dedicated lqNMR spectrometer.<sup>[17]</sup> For liquid species where Brownian motion occurs, the anisotropic parts of the NMR interactions are canceled by the random orientation of substances in liquid media. Only the interactions with non-zero isotropic parts are detected in the NMR spectrum (i.e., chemical shift and scalar couplings), resulting in narrow NMR peaks (a few-Hz peak width) in a lqNMR spectrum. For solid species where Brownian motion is strongly limited, anisotropic NMR interactions lead to a significant broadening of the NMR peak. Resolved ssNMR peaks with a few kHz width can only be obtained using the magic-angle spinning (MAS) technique, which spins a rotor containing the specimen around an axis tilted by 54.7° from the static magnetic field axis.<sup>[18–20]</sup>

For heterogeneous samples such as suspension, gel, tissues, cells, an additional source of line broadening comes from the magnetic susceptibility gradient.<sup>[21]</sup> The magnetic susceptibility factor describes the sample's permeability to the magnetic field. The higher the magnetic susceptibility, the higher the magnetic field created in the sample induced by the external magnetic field.<sup>[21]</sup> Samples placed in different homogenous liquid media have several discrete chemical shifts. In the case of a heterogeneous medium, different interfaces between the sample and the medium cause varied magnetic susceptibility. Also, a gradient of distance-dependent dipolar coupling between solvent and sample nuclear spin causes a gradient of chemical shift. These two effects combine into broad signals in the resulting NMR spectra.<sup>[21]</sup> This line broadening due to heterogeneity can be reduced by using MAS.<sup>[21]</sup> Sometimes, a spinning rate of only a few kHz is sufficient to average this magnetic susceptibility.<sup>[22]</sup> This phenomenon is behind the concept of HR-MAS NMR for semisolids. In a simplified way, HR-MAS is the marriage of lqNMR and ssNMR, using the MAS technique to obtain high-resolution lqNMR-like spectra. Compared to MAS NMR for solids, HR-MAS NMR for semisolids needs specifically designed probes with magnetic gradient coil.<sup>[23,24]</sup> Liquid-like samples are packed in inserts to prevent sample dehydration or liquid leakage into the spectrometer.

Different uses of *in-situ* NMR spectroscopy in drug delivery have been reported, taking into account the heterogeneity of the system. Westesen et al. used <sup>1</sup>H lqNMR to characterize the state of several poorly water-soluble drugs incorporated in lipid NPs.<sup>[25]</sup> The loaded drug changed from mobile (narrow line width) in lipid emulsion to confined (broad line width and signal intensity decrease) in lipid suspension. A similar principle was used to assign the <sup>13</sup>C cross-polarization (CP) MAS NMR spectra of poly-n-butylcryanoacrylate nanocapsule suspension in water.<sup>[26,27]</sup> In another study combining the use of MAS-NMR, lqNMR, and HR-MAS NMR, the structural organization of nanocrystal suspension of carbamazepine (CBZ) and CBZ-saccharin was investigated in various media.<sup>[28]</sup> More importantly, Kenneth's group developed different NMR methods to monitor *in-situ* several dynamic processes. Firstly, they used solid-state <sup>13</sup>C CPMAS NMR spectroscopy to monitor the crystallization of two glycine polymorphs from its solution.<sup>[29]</sup> Later, they reported a

method to detect both solid and liquid phases, by using a home-made NMR pulse program combining two different pulse sequences for solid- and liquid-NMR measurements alternatively.<sup>[30]</sup> These *in-situ* NMR methods have been applied to study crystallization processes of several polymorphs.<sup>[17]</sup> In 2021, the same group attempted to record the species' evolution at both solid and liquid phases during the formation of a nickel metal-organic framework (MOF) using ssNMR.<sup>[31]</sup> *In-situ* <sup>31</sup>P NMR showed the disappearance over time of the organic ligands in the liquid phase. *In-situ* <sup>1</sup>H NMR data demonstrated organic linkers' deprotonation and metal coordination during MOF nucleation and growth, providing insight on the crystallization kinetics and the process's activation energies.

To our knowledge, no *in-situ* NMR studies of DDSs yet can simultaneously monitor species from different phases. Herein, we propose an *in-situ* NMR protocol for the investigation of the degradation reaction of MOF NPs (nanoMOFs) in biological-mimicking media, as well as drug release. MOF, a porous coordination network between metal and chelating organic ligands, offers high drug loading capacity and versatile modification.<sup>[32,33]</sup> We chose nanoMIL-100(Al) (MIL stands for material of Institute Lavoisier) as a model DDS for its well-established degradation reaction forming both solid and liquid products.<sup>[34,35]</sup> In addition, the degradation products, trimesic acid and aluminophosphate, can be identified through sensitive NMR nuclei, such as <sup>1</sup>H and <sup>27</sup>Al. This paper presents i) the new *in-situ* NMR methodology to monitor species at liquid and solid phases at the same time, ii) the proof of concept of *in-situ* NMR for studying the degradation of nanoMIL-100(Al) and its structural analog nanoMIL-100(Fe), and iii) the application of *in-situ* NMR method for the drug-loaded nanoMIL-100(Al). Our *in-situ* NMR method was able to demonstrate the degradation mechanism of nanoMIL-100(Al) and nanoMIL-100(Fe) in qualitative and quantitative manners. This method also allowed us to study the effect of drug encapsulation on nanoMIL-100 degradation reaction, and provided important information about the drug delivery processes in this system.

## 2. Results and Discussions

### 2.1. MOFs Synthesis

DLS measurements of as-synthesized nanoMIL-100(Fe) in EtOH showed a mean hydrodynamic diameter of 230 ± 20 nm and a polydispersity index (Pdl) of 0.13 ± 0.03, while nanoMIL-100(Al) gave after purification a mean hydrodynamic diameter of 150 ± 10 nm and Pdl of 0.10 ± 0.02. TEM images in Figure 1 also display the two nanoMIL-100 particles in EtOH suspension with uniform shape and size. The two MIL-100 MOFs display a type II N<sub>2</sub> adsorption isotherm (Figure 1). Two uptakes at P/P<sub>0</sub> of 0.05 and 0.12 were usually explained by the presence of two types of cages with different pore sizes and pore-opening windows. They also have the same high BET surface area of 1600 ± 300 m<sup>2</sup> g<sup>-1</sup>. The as-synthesized nanoMIL-100(Al) and nanoMIL-100(Fe) have similar experimentally measured XRD patterns (Figure 1), as expected from their analogue crystal structure.

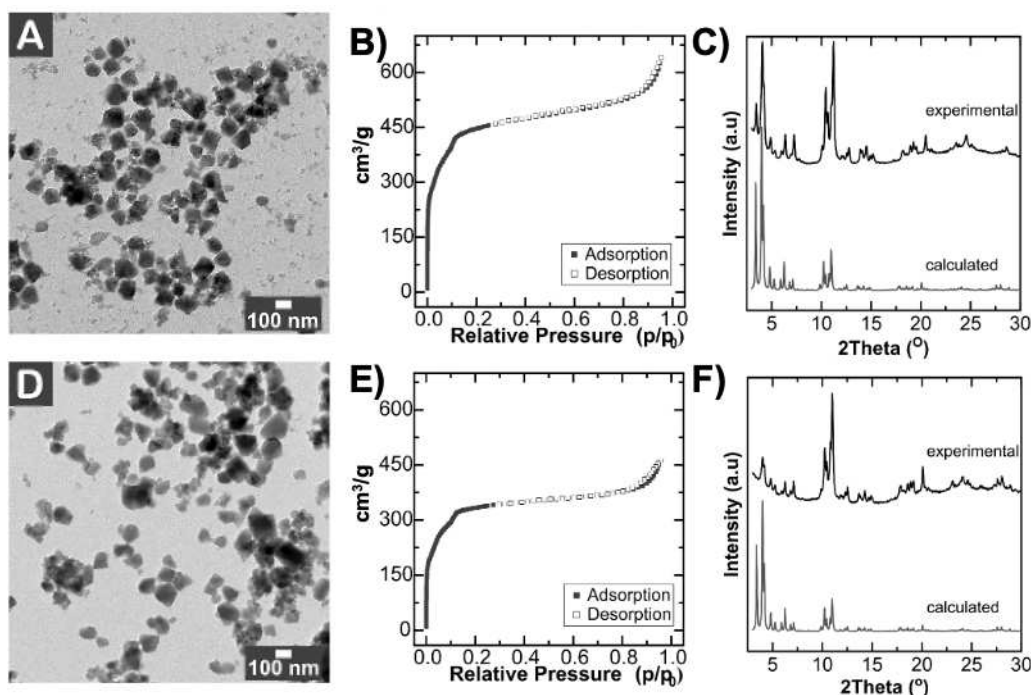


**Figure 1.** (A, D) TEM images, (B, E)  $N_2$  adsorption isotherm, and (C, F) experimental and calculated XRD patterns of (A–C) nanoMIL-100(Al) and (D–F) nanoMIL-100(Fe), respectively.

Also, the position and the width of the main diffraction peaks are similar to those in the calculated XRD pattern obtained from MOF crystal, testifying to the high crystallinity of the as-synthesized MOF. The difference between the relative intensities of their diffraction peaks is due to the preferential orientations of the nanocrystallites.

## 2.2. Set Up In-Situ NMR Method

The major challenge that previous *in-situ* NMR studies of NP suspension face, is to get an adequate resolution for both liquid and solid-phase NMR signals. In the chosen case study, degradation of iron/aluminum trimesate nanoMIL-100, as studied recently,<sup>[34,35]</sup> produces free solvated trimesate in solution and the remaining coordinated trimesate ligand in solid form. As the solid- and liquid-state substances have distinctive characteristic NMR features and behaviors, they are normally measured by separate NMR techniques. The trimesic acid solution has a narrow NMR signature peak of 1–2 Hz width, while trimesic acid powder has a broad peak of 50–100 Hz width under a MAS rate of 10–15 kHz. Usually, HR-MAS NMR spectroscopy, which requires only a moderate MAS rate, produces high-quality measurements of the liquid phase in soft matters and heterogeneous media. However, this strategy is unsuitable for efficiently probing solid-phase components, especially when high resolution is needed.

The effect of the spinning rate on the NMR spectra quality is demonstrated in Figure 2. We measured MAS NMR spectra of nanoMIL-100(Al) suspension in phosphate buffer at different

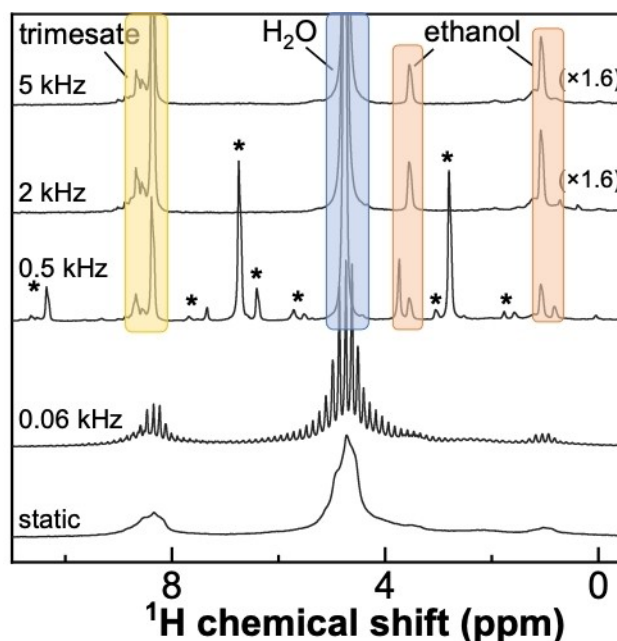


**Figure 2.**  $^1H$  MAS NMR spectra of nanoMIL-100(Al) suspension in phosphate buffer (PB) recorded at different MAS rates. Spinning side bands are indicated by asterisks, and resonances of trimesate, water and ethanol are highlighted by yellow, blue and red rectangles.

MAS rates. The higher the spinning rate, the more resolved the NMR peaks and the more reduced the spinning sidebands are. When there is no spinning (static), the signals are broad, and no information can be deduced. Generally, static NMR measurement of a pure liquid or a diluted suspension yields signals of

species at the liquid phase, which should be narrow (line width of a few Hz). However, the investigated suspension of nanoMIL-100 is highly concentrated and heterogeneous. Due to the gradient of magnetic susceptibility, the obtained NMR peaks of liquid-phase species are also broad, like those of a pure solid-state sample.<sup>[21]</sup> Therefore, a certain MAS rate is required to average this magnetic susceptibility and to increase the resolution of solid species' signals.

At a very slow rotation speed of 60 Hz (measured from sidebands spacing), multiple spinning sidebands clutter the NMR spectrum, making it impossible to distinguish the overlapping signals. Raising the MAS rate to 0.5 or 2 kHz significantly improved the NMR spectrum quality, where narrow lines from the liquid phase are now clearly visible. Still, at 0.5 kHz MAS, the intensity of the isotropic signal is not maximized, and at 2 kHz, a few spinning sidebands are now close to the peaks of interest. We found that the minimum MAS rate needed for acceptable NMR spectra quality is 5 kHz. We decided on the MAS rate of 10 kHz to have sufficient <sup>27</sup>Al NMR resolution for solid-state species and to get a temperature inside the sample rotor of 34 °C,<sup>[36]</sup> close to the human body temperature of 37 °C. Note that a similar effect of MAS on the NMR spectra of nanoMIL-100(Fe) suspension was observed (data not shown), even though only signals of liquid species were detectable here.

The second issue to be solved is choosing the MOF degradation condition for *in-situ* NMR study. The NMR rotor-insert system has a maximum volume capacity of 25 μL (see experimental section), dramatically smaller than the volume used for the *ex-situ* NMR study. Other constraints are to get decent NMR sensitivity for both solid and liquid trimesate. The input MIL-100(Al) weight should be at least a few mg. On the other hand, the input phosphate buffer saline (PBS)/Al ratio must be high enough to trigger release sufficient liquid trimesate.<sup>[34,35]</sup> Therefore, to miniaturize the laboratory-scale degradation condition, concentrated phosphate buffer (PB) was used to match the input MOF reactant. In addition, PB was prepared in deuterated water D<sub>2</sub>O to avoid the signal of water as much as possible. Also, no NaCl salt was added to PB as the required salt concentration of concentrated phosphate buffer saline exceeds their solubility. Under such dilute conditions, it was difficult to record <sup>13</sup>C experiments within reasonable timescale and with sufficient spectral quality.

The pulse program parameters (mainly number of scans, relaxation delays, and acquisition times) for NMR were optimized to observe the most NMR signals of solid and liquid substances as well as to satisfy the quantitative NMR's requirements. The optimization of <sup>1</sup>H or <sup>27</sup>Al NMR measurement parameters was done on a solid-liquid mixture of nanoMIL-100(Al) powder with trimesic acid solution and/or aluminum nitrate solution, respectively. The final values are reported in the experimental section.

Finally, there are three ways to conduct *in-situ* NMR measurements reported in the literature: simultaneous, alternating, and sequential NMR. Simultaneous NMR<sup>[37]</sup> which can record NMR signals up to four NMR nuclei at the same time, offer the most accurate time-resolved NMR measurement.

However, this acquisition method was difficult to set up in the current study because of the different nature of the two NMR nuclei types used here, <sup>1</sup>/<sub>2</sub>-spin <sup>1</sup>H versus quadrupolar <sup>27</sup>Al, that require too different optimal experimental NMR parameters (number of scans, acquisition times, relaxation delays, etc.). Alternating acquisition<sup>[30]</sup> offers independent implementation of solid-selective and liquid-selective pulse sequences, yet, only one nucleus can be recorded once at a time. In comparison, sequential NMR measurement records a series of 1D NMR experiments alternating between two nuclei in separate channels,<sup>[31]</sup> making it relatively easy to set up. This later was found the most appropriate method for our system.

### 2.3. In-Situ NMR Study of NanoMOF Degradation

Figure 3 shows *in-situ* NMR spectra acquired during degradation of the nanoMIL-100(Al) suspension in PB. It was possible to observe the signature of both solid-state and liquid-state trimesate by <sup>1</sup>H NMR (Figure 3A), assigned to the peaks with linewidths more than 200 Hz and the peaks with linewidths 50–70 Hz, respectively. The <sup>1</sup>H NMR spectra series reveals an increase of liquid trimesate peaks and a decrease of solid trimesate peaks. This phenomenon fits well with the proposed trimesate release mechanism due to the cleavage of coordinated trimesate ligands.<sup>[34,35]</sup> This *in-situ* NMR method results in acceptable quality for <sup>1</sup>H NMR spectra and, more importantly, conservation of the total liquid and solid trimesate peak area after 48 h, thus, these NMR measurements are quantitative. The fluctuation in the area of <sup>1</sup>H NMR signals varies within a range of 3% throughout the 48 h of experimentation. On the other hand, the *in-situ* <sup>27</sup>Al NMR spectra (Figure 3B) show the decrease of the peak representing the original Al species connected with trimesate ligand Al–O–C and the increase of the peak representing degraded Al species connected with phosphate Al–O–P. This is fully consistent with previous *ex-situ* study results.<sup>[34,35]</sup>

As a comparison, *in-situ* lqNMR measurement was also performed on the nanoMIL-100(Al) suspension with the same

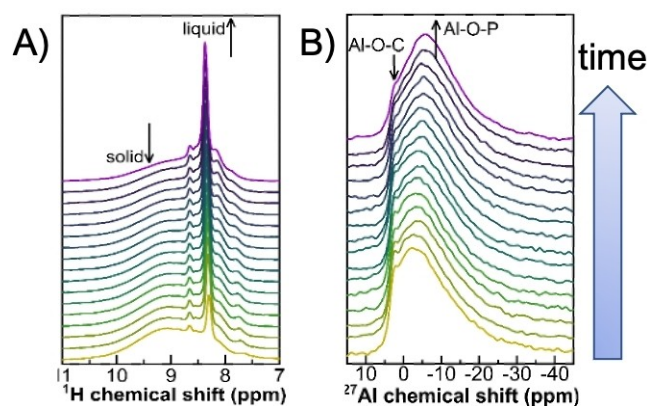
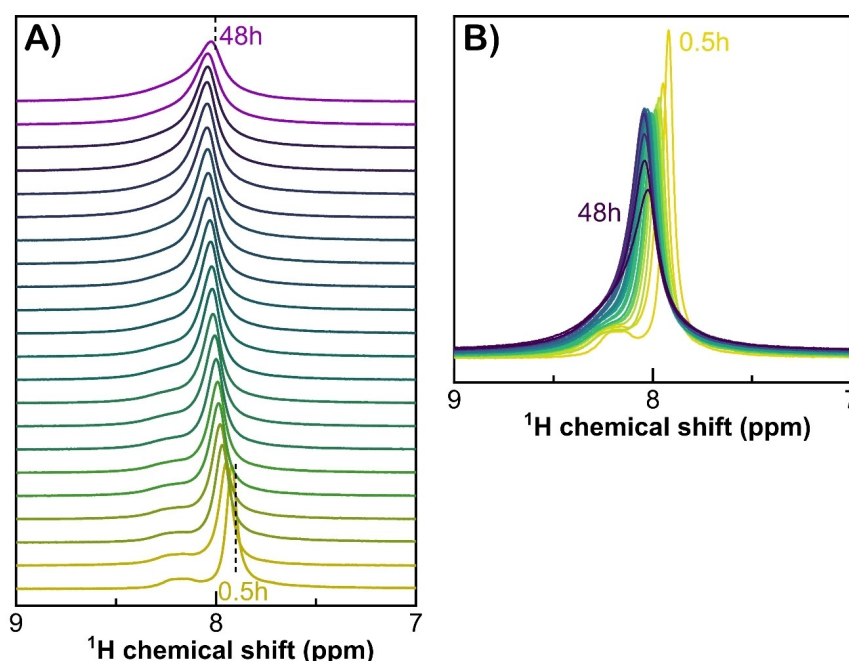


Figure 3. *In-situ* (A) <sup>1</sup>H and (B) <sup>27</sup>Al MAS NMR spectra recorded as a function of time over 48 h of nanoMIL-100(Al) degradation in PB. Conditions: 5 mg MOF + 25 μL PB-D<sub>2</sub>O 400 mmol L<sup>-1</sup>.

PB/Al ratio as *in-situ* MAS NMR. Figure 4 displays the  $^1\text{H}$  NMR series obtained with 120 mg MOF in 600  $\mu\text{L}$  PB- $\text{D}_2\text{O}$  400  $\text{mmol L}^{-1}$  using a conventional 5-mm glass NMR tube in static condition. In the beginning (Figure 3B), there were two peaks, a narrow peak representing released trimesate and a small broad peak, signaling suspension precipitation. As degradation went on, these two peaks gradually converged into one moderately broad peak. Due to this precipitation and the fact that lqNMR misses the signal from solid species, the total trimesate peak area was not well conserved (peak area variation of 35%). *In-situ* lqNMR neither observed trimesate in the solid phase nor allowed quantification of trimesate formation. Addi-

tionally, it could not detect any substantial signal of  $^{27}\text{Al}$  (data not shown), indicating that no  $\text{Al}^{3+}$  species were released into the solution phase. This experiment demonstrates that MAS NMR is versatile and well adapted for the *in-situ* NMR study of MOF degradation because it is a unique tool to detect trimesate degradation products in both solid and liquid phase.

From *in-situ* MAS NMR measurement, one can plot the kinetics of the MIL-100 degradation reaction (Figure 5) by deconvoluting the peak area of solid-phase and liquid-phase trimesate species. As their total peak area is more or less conserved over time (3% fluctuation), it is considered to represent 100% of trimesate in the sample. The proportion of



**Figure 4.** *In-situ*  $^1\text{H}$  lqNMR spectra recorded as a function of time over 48 h of nanoMIL-100(Al) degradation in PB using 5-mm glass NMR tube. Condition: 120 mg MOF + 600  $\mu\text{L}$  PB- $\text{D}_2\text{O}$  400  $\text{mmol L}^{-1}$ .

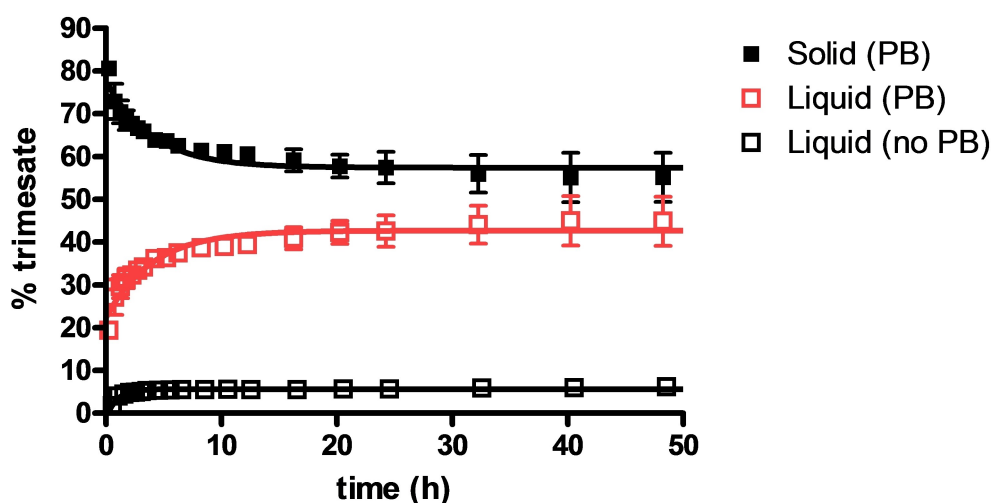


**Figure 5.** Kinetics of nanoMIL-100(Al) degradation in phosphate (PB- $\text{D}_2\text{O}$ ): trimesate ligand release in the liquid phase (empty square) and ligand loss in the solid phase (filled square), in comparison with ligand release when incubating nanoMIL-100(Al) in  $\text{D}_2\text{O}$  (control experiment). The curves represent first-order kinetic models. Reaction condition: 5 mg nanoMOF + 25  $\mu\text{L}$  PB- $\text{D}_2\text{O}$  400  $\text{mmol L}^{-1}$  or 25  $\mu\text{L}$   $\text{D}_2\text{O}$ .

trimesate in the solid and liquid phases is then calculated by the relative ratio to the total trimesate peak area. Notably, the trimesate release profile obtained from *in-situ* NMR has a similar shape to the one obtained from *ex-situ* NMR and HPLC experiments we reported previously.<sup>[34,35]</sup> Under the degradation condition here, 45% of free trimesate was formed after 48 h, corresponding to 55% of trimesate loss of original MIL-100(Al). Less than 6% standard deviation was obtained from two different synthesis batches of MOF, demonstrating that the *in-situ* measurement was reproducible. *In-situ* degradation with pure deuterated water was also performed as a control experiment, leading to only 6% release of trimesate after 48 h. In addition, the data were analyzed quantitatively by considering first-order kinetic models to extract degradation rates under these conditions. While degradation is very limited in pure water, ligand release was faster ( $k=1.1\pm 0.1\text{ h}^{-1}$ ) than in PB, with a release rate of  $k=0.25\pm 0.04\text{ h}^{-1}$ . These results show that in a phosphate environment, degradation is slow, progressive and highly efficient. Overall, it is feasible to use *in-situ* NMR for the quantitative study of NPs suspension, which could save labor and time as compared to *ex-situ* studies when one need to extract samples after each time point.

On top of revealing what happens to the organic ligands during the degradation reaction in qualitative and quantitative fashions, *in-situ* NMR gives information about the evolution of the metal's coordination sphere. *In-situ*  $^{27}\text{Al}$  NMR spectra (Figure 3B) show the signature of degradation in metal coordination. Like  $^1\text{H}$  NMR,  $^{27}\text{Al}$  NMR observes a declining signal and a rising signal. The declining signal belongs to the Al species in the original MOFs, the Al connected with trimesate ligand. The rising signal is associated with the degraded Al species connected with phosphate. Not only 6-coordinate aluminophosphate but also 4-coordinate aluminophosphate was observed at 48 ppm. This result from *in-situ* NMR agrees with our previous *ex-situ* ssNMR data.<sup>[34,35]</sup>

The degradation kinetics of nanoMIL-100(Fe) was also studied in the same way. The resulting time-resolved NMR spectra are reported in Figure 6A. Contrasting to the *in-situ*  $^1\text{H}$  NMR spectra of MIL-100(Al), those of MIL-100(Fe) only consist of an increasingly narrow peak representing the liquid-phase trimesate. The peak of solid-phase trimesate was not visible as it directly bonds to paramagnetic Fe(III). The liquid trimesate signal from nanoMIL-100(Fe) degradation is however observable and has a line width similar to that from nanoMIL-100(Al) indicating that negligible or no free  $\text{Fe}^{3+}$  cations were formed during MIL-100(Fe) degradation. The area of the  $^1\text{H}$  peak as a function of time is shown in Figure 6B, which exhibits a similar trend to the liquid trimesate release curve with aluminum-analog nanoMOF (see Figure 5). However, the trimesate release rate constant  $k=0.5\pm 0.1\text{ h}^{-1}$ , is twice as large as the value obtained with the MIL-100(Al) under the same conditions. The degradation process is therefore faster with MIL-100(Fe) than with the aluminum analog, although this does not necessarily mean that Fe-nanoMOF degradation is more advanced than its aluminum counterpart.

In summary, a proof-of-concept for *in-situ* NMR method for NPs suspension was obtained. An example case study of nanoMOF degradation was demonstrated. This *in-situ* NMR technique can monitor the reaction products both at liquid and solid phases simultaneously, as well as offer both qualitative and quantitative analysis.

#### 2.4. In-Situ NMR Study of Drug-Loaded NanoMOF Degradation

Here, we demonstrate that the established *in-situ* NMR technique could provide information about drug release mechanisms. As a proof-of-concept, nanoMIL-100(Al) was loaded with the two drugs previously studied, adenosine

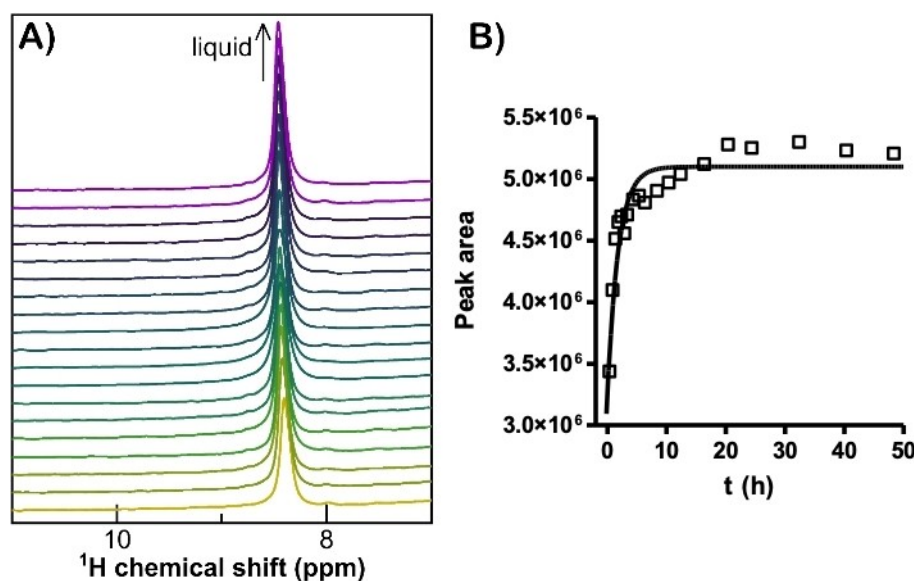


**Figure 6.** (A) *In-situ*  $^1\text{H}$  MAS NMR spectra and (B) peak area as a function of time over 48 h of nanoMIL-100(Fe) degradation in PB. The curve corresponds to the best fit of experimental data with a first-order kinetic model. Condition: 5 mg MOF + 25  $\mu\text{L}$  PB- $\text{D}_2\text{O}$  400  $\text{mmol L}^{-1}$ .

triphosphate (ATP) and monophosphate (AMP).<sup>[34,35]</sup> Then, the drug-loaded MOFs, ATP@nanoMIL-100(Al) and AMP@nanoMIL-100(Al) were degraded in PB (2 mg MOF + 25 mL PB 1 mol L<sup>-1</sup>).

*In-situ* NMR kinetics experiments were performed. <sup>1</sup>H NMR spectra presented in Figure 7 gave information about the drug release process. First, in both <sup>1</sup>H NMR spectra of ATP- and AMP-loaded nanoMIL-100(Al), the progressive apparition of released liquid trimesate and coordinated solid trimesate was similar to what has been observed for the degradation of empty nanoMIL-100(Al) described in section 2.2. Furthermore, in the spectra of degraded AMP@nanoMIL-100(Al) in Figure 7A, a signal of AMP was found at 6 ppm, corresponding to the proton of the sugar ring's CH- group connecting to the adenosine.<sup>[38]</sup> This peak has a line width of 50–70 Hz, which is relatively small to the peak of solid trimesate. Therefore, it was assigned to the liquid-state AMP released from the AMP@MOF. On the opposite, there was no peak at 6 ppm<sup>[38]</sup> in the <sup>1</sup>H NMR spectra of degraded ATP@nanoMIL-100(Al) (Figure 7B), consistent with our previous findings that ATP@nanoMIL-100(Al) is less degradable than the AMP-loaded counterpart due to its stronger drug-carrier connection.<sup>[34,35]</sup> Note that other signals of AMP and ATP in the aromatic region overlapped with the signal of nanoMIL-100(Al)'s trimesate ligands, making it difficult to determine both the ligand and drug release.

Likewise, this difference between the degradation of ATP- and AMP-loaded MOF was reflected in the <sup>27</sup>Al NMR measurement results (Figure 8). In both cases, a decrease of the Al–O–C trimesate peak at around 0 ppm and an increase of the 6-coordinate Al–O–P peak at around –12 ppm were observed. In addition, the appearance of the 4-coordinate Al–O–P at 48 ppm was noticeable.<sup>[39]</sup> The proportion of this degraded Al over the total Al in the sample was estimated by peak integration. Figure 9 shows that the formation rate of this degradation

product was faster in the case of AMP-loaded nanoMIL-100(Al) than the ATP-loaded one. As ATP with the triphosphate group is slightly more strongly complexed with Al(III) than its monophosphate AMP analog,<sup>[40]</sup> it is more difficult for the inorganic phosphate in PB to displace ATP. Consequently, the degradation and the drug release process are easier and more pronounced with AMP@MIL-100(Al) as indicated by the greater amount of degraded 4-coordinated Al species (<sup>27</sup>Al NMR in Figure 8) and released drug (<sup>1</sup>H NMR in Figure 7).

### 3. Conclusions

The present study proposes for the first time a versatile *in-situ* NMR spectroscopy method for monitoring both drug release and degradation processes of MOF nanocarriers. Without the need of separating NP suspension, both qualitative and quantitative information about the mechanism and kinetics of carrier degradation can be achieved.

After setting up *in-situ* MAS NMR method using commercially available instruments, we demonstrate the proof-of-concept of *in-situ* NMR for studying a MOF-based drug delivery system, MIL-100(Al) NP suspension. The present method was able to evidence the nanoMIL-100(Al) degradation reaction mechanisms in phosphate media. Both the kinetics of ligand release in the liquid phase and the evolution in nanoMIL-100(Al)'s coordination environment could be detected and followed simultaneously. In addition, we demonstrated that this method could be useful for MOFs made of paramagnetic iron like nanoMIL-100(Fe). Information from the liquid NMR species was useful for quantitative measurement. *In-situ* NMR was further exploited to gain information on the release processes of two drugs from nanoMIL-100(Al).

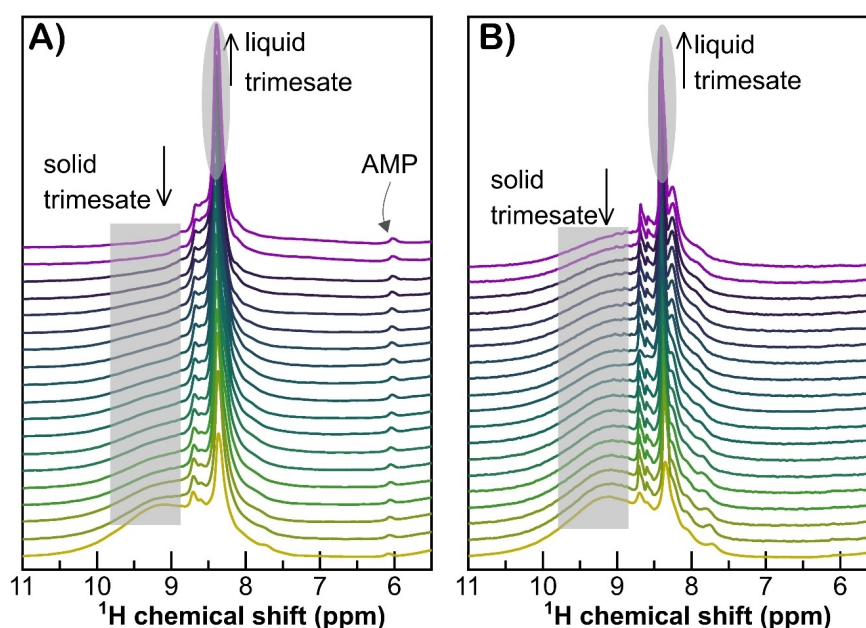


**Figure 7.** *In-situ* <sup>1</sup>H MAS NMR spectra recorded as a function of time over a period of 48 h during the degradation of nanoMIL-100(Al) loaded with (A) AMP, and (B) ATP. Condition: 2 mg MOF + 25  $\mu$ L PB-D<sub>2</sub>O 1 mol L<sup>-1</sup>.

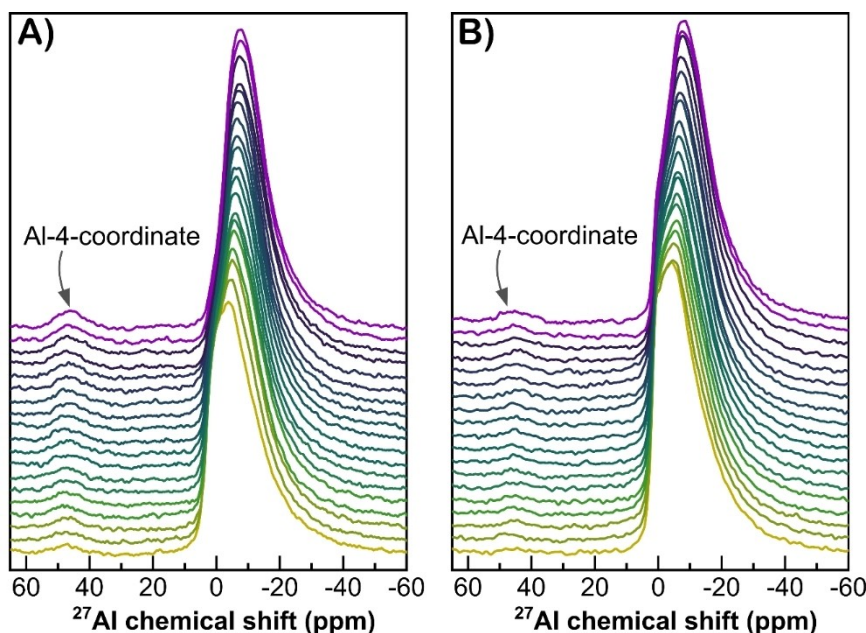


Figure 8. *In-situ*  $^{27}\text{Al}$  MAS NMR spectra recorded as a function of time over a period of 48 h during the degradation of nanoMIL-100(Al) loaded with (A) AMP, and (B) ATP. Condition: 2 mg MOF + 25  $\mu\text{L}$  PB- $\text{D}_2\text{O}$  1  $\text{mol L}^{-1}$ .

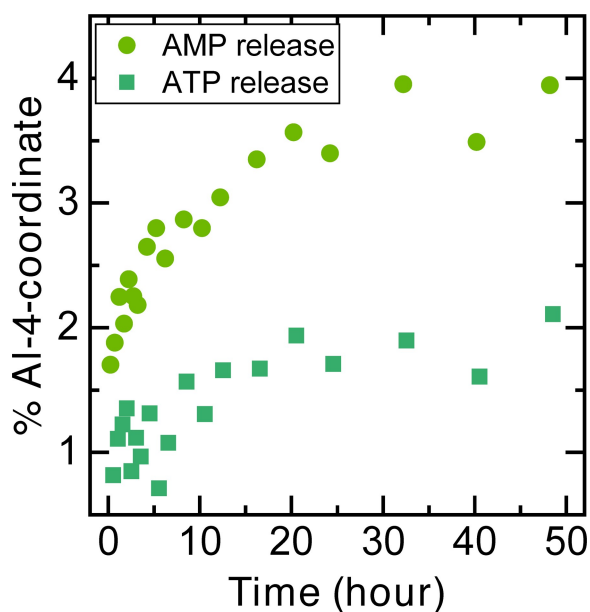


Figure 9. Proportion of Al-4-coordinate formed during drug release, i.e., degradation of ATP- and AMP-loaded nanoMIL-100(Al).

The *in-situ* NMR spectroscopy described in this work can be used as a framework for other types of nanocarriers/colloidal systems or other reactions taking place in NP suspensions.

## Experimental Section

All reagents and solvents were used without any purification. The drug solutions were prepared from ATP disodium hydrate salt or AMP sodium hydrate salt.

## NanoMIL-100 Synthesis and Characterization

NanoMIL-100(Al) and nanoMIL-100(Fe) were synthesized by microwave synthesis technique.<sup>[41,42]</sup> Particle size distribution was analyzed by dynamic light scattering (DLS) in a Zetasizer Nano ZS90 instrument from Malvern Panalytical. Morphology and size of 0.5  $\text{mg mL}^{-1}$  nanoMOF suspension were observed by transmission electron microscopy (TEM) under a 120 kV JEOL JEM-1400 microscope. Crystallinity of MOF powder was checked by powder X-ray diffraction (PXRD) at  $\lambda(\text{Cu K}\alpha)$  of 1.5406  $\text{\AA}$ , using a Siemens D5000 diffractometer. Porosity of MOF was evaluated from the nitrogen gas adsorption measured by a Micromeritics Tristar II Plus.

## Degradation of NanoMIL-100

A small-volume reaction between nanoMIL-100 and phosphate buffer was carried out to adapt for the NMR insert needed for *in-situ* NMR measurement. Basically, in a round-bottom 2 mL Eppendorf tube, 5 mg of MOF was mixed with 25  $\mu\text{L}$  phosphate buffer (PB) in deuterated water ( $\text{D}_2\text{O}$ ).

The phosphate buffer in deuterated water (PB- $\text{D}_2\text{O}$ ) was prepared as follows. The stock solution of  $\text{KH}_2\text{PO}_4$  1  $\text{mol L}^{-1}$  (stock A) was prepared by dissolving 1.36 g of the anhydrous salt in 10 mL  $\text{D}_2\text{O}$ . For the stock solution of  $\text{Na}_2\text{HPO}_4$  1  $\text{mol L}^{-1}$  (stock B), portion by portion of the anhydrous salt was gradually added to  $\text{D}_2\text{O}$  under vigorous stirring and heating at 35–45  $^\circ\text{C}$  in a water bath. Afterward, to get PB- $\text{D}_2\text{O}$  1  $\text{mol L}^{-1}$ , one gradually pipettes 2.8 mL stock A to 7.7 mL stock B. The stock solutions and PB were stored at room temperature.

Prior to the degradation reaction, 5 mg wetted MOF pellet was obtained by centrifugation (11 000 RCF for 15 min) from its stock suspension in ethanol absolute (EtOH abs). Then, the pellet was washed twice in  $\text{D}_2\text{O}$  as follows: the wet pellet was carefully redispersed in 100  $\mu\text{L}$   $\text{D}_2\text{O}$  first (hand shaking and gentle vortex), then 1 mL  $\text{D}_2\text{O}$  was added, and the suspension was mixed again.  $\text{D}_2\text{O}$  was removed by centrifugation (10 000 RCF for 10–15 min) to get a clear and non-blurry supernatant. After the last centrifugation

step, the supernatant should be discarded as much as possible. Finally, 25  $\mu\text{L}$  of  $\text{PB-D}_2\text{O}$  400  $\text{mmol L}^{-1}$  was added to the Eppendorf tube. The suspension in PB was dispersed rapidly by vortexing. 25  $\mu\text{L}$  of this suspension was injected into the NMR insert (Figure 10) by using a pipette. The insert was sealed by a screw cap and then placed inside the NMR rotor for subsequent NMR measurements.

### Drug Loading of NanoMIL-100 and Drug Release

The drug loading procedure reported in the previous publication<sup>[34,35]</sup> was adapted to prepare a small volume of samples. Briefly, 5  $\text{mg mL}^{-1}$  MOF suspension was mixed with 1.5  $\text{mg mL}^{-1}$  drug solution, corresponding to 30 wt% input drug loading. The volume of the drug solution was determined from the needed weight of MOF. The removal of EtOH abs and washing with  $\text{D}_2\text{O}$  were carried out in the same way as described in the degradation experiment. The purification procedure can be scaled up if necessary. After the washing step, 100  $\mu\text{L}$  of 1.5  $\text{mg mL}^{-1}$  ATP or AMP drug solution was added to the wet MOF pellet first, and the mixture was dispersed by hand shaking. Then, the remaining drug solution was added, and the mixture was dispersed by hand shaking and pipetting. Finally, the suspension was subjected to continuous shaking overnight at room temperature.

For the drug release experiment on the next day, 2 mg of drug-loaded MOF was recovered from the drug loading suspension by centrifuging at 10 000 RCF for 10 min. The obtained pellet was washed with 1 mL  $\text{D}_2\text{O}$ , which was later removed by centrifuging at 10 000 RCF for 10 min. The supernatant should be discarded as much as possible. Finally, the wet MOF pellet was redispersed in 25  $\mu\text{L}$  of  $\text{PB-D}_2\text{O}$  1  $\text{mol L}^{-1}$ , and the obtained mixture was placed in an NMR insert as in the degradation experiment. *In-situ* NMR measurements were then carried out as quickly as possible.

### In-Situ NMR Spectroscopy

Solid-state NMR experiments were performed at 11.7 T on a Bruker NEO NMR WB spectrometer equipped with a 4 mm probe head. MAS was applied at 10 kHz. For spinning samples, the suspension was contained in a Bruker disposable insert purchased from Cortecnet. These inserts provide a tight seal to prevent dehydration or loss of solvent during MAS experiments. The 25  $\mu\text{L}$  disposable Kel-F® inserts use a plug and screw cap and can fit standard Bruker BioSpin 4 mm rotors (Figure 10). For reuse, the sample inside the insert was removed by adsorption on dry paper. Then, the insert was sonicated separately in ethanol, acetone, and water. Finally, the insert was dried in the oven at 30 °C.

Sequential NMR measurement was performed by direct excitation. At each time point, the acquisition of the  $^1\text{H}$  signal was followed immediately by  $^{27}\text{Al}$ . Kinetics measurement was programmed using a variable delay (from 0.5 to 8 h) placed after data acquisition in the  $^{27}\text{Al}$  pulse sequence. The acquisition parameters were, for  $^1\text{H}$  NMR: a pulse of 3.35  $\mu\text{s}$  length and 100 W power, acquisition time of 1.6 s, recycling delay of 4.4 s, and total experimental time of ca. 3 min,

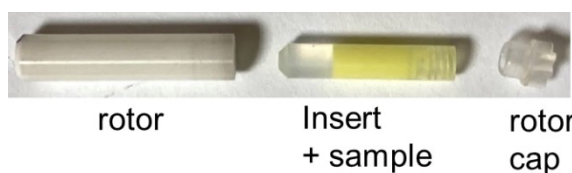


Figure 10. Photo of insert-rotor ensemble used for *in-situ* NMR experiments.

and for  $^{27}\text{Al}$  NMR: a pulse of 3.5  $\mu\text{s}$  length and 40 W power, acquisition time of 0.01 s, recycling delay of 0.1 s, and total experimental time of ca. 27 min.

*In-situ*  $^1\text{H}$  NMR spectroscopy was performed at 9.4 T on a Bruker Avance spectrometer equipped with a probe head of 5 mm. The  $^1\text{H}$  NMR experiments were recorded with a pulse length of 8  $\mu\text{s}$ , a waiting time between two consecutive scans of 6 s, and total experimental time of ca. 30 s.

All NMR experiments were conducted at 37 °C for *in-situ*  $^1\text{H}$  NMR and 34 °C for *in-situ* MAS NMR. The chemical shifts were referenced to tetramethylsilane for  $^1\text{H}$ , and to  $\text{Al}(\text{NO}_3)_3$  1  $\text{mol L}^{-1}$  solution for  $^{27}\text{Al}$ .

### Acknowledgements

This work was supported by the Paris Ile-de-France Region – DIM “Respire”, and a public grant overseen by the French National Research Agency as part of the “Investissements d’Avenir” program (Labex Charm3at, ANR-11-LABX-0039-grant).

### Conflict of Interests

The authors declare no conflict of interest.

### Data Availability Statement

The data that support the findings of this study are available from the corresponding author upon reasonable request.

**Keywords:** *in-situ* NMR spectroscopy · drug delivery · nanoMOF · degradation · MIL-100

- [1] S. Talebian, T. Rodrigues, J. das Neves, B. Sarmiento, R. Langer, J. Conde, *ACS Nano* **2021**, *15*, 15940.
- [2] M. J. Mitchell, M. M. Billingsley, R. M. Haley, M. E. Wechsler, N. A. Peppas, R. Langer, *Nat. Rev. Drug Discovery* **2021**, *20*, 101.
- [3] O. C. Farokhzad, R. Langer, *ACS Nano* **2009**, *3*, 16.
- [4] A. Akinc, *Nat. Nanotechnol.* **2019**, *14*, 4.
- [5] J.-B. Coty, C. Vauthier, *J. Controlled Release* **2018**, *275*, 254.
- [6] J. D. Clogston, *Adv. Drug Delivery Rev.* **2021**, *176*, 113897.
- [7] M. A. Younis, H. M. Tawfeek, A. A. H. Abdellatif, J. A. Abdel-Aleem, H. Harashima, *Adv. Drug Delivery Rev.* **2022**, *181*, 114083.
- [8] J. Mathurin, E. Pancani, A. Deniset-Besseau, K. Kjoller, C. B. Prater, R. Gref, A. Dazzi, *Analyst* **2018**, *143*, 5940.
- [9] J. Penders, I. J. Pence, C. C. Horgan, M. S. Bergholt, C. S. Wood, A. Najer, U. Kauscher, A. Nagelkerke, M. M. Stevens, *Nat. Commun.* **2018**, *9*, 4256.
- [10] C. L. McFearn, J. Sankaranarayanan, A. Almutairi, *Anal. Chem.* **2011**, *83*, 3943.
- [11] S. Bou, A. S. Klymchenko, M. Collot, *ACS Appl. Nano Mater.* **2022**, *5*, 4241.
- [12] N. Artzi, N. Oliva, C. Puron, S. Shitreet, S. Artzi, A. B. Ramos, A. Groothuis, G. Sahagian, E. R. Edelman, *Nat. Mater.* **2011**, *10*, 704.
- [13] S. G. Kazarian, K. L. A. Chan, *Macromolecules* **2003**, *36*, 9866.
- [14] G. Cinar, C. Englert, M. Lehmann, I. Nischang, *Anal. Chem.* **2020**, *92*, 7932.
- [15] C. L. McFearn, J. Sankaranarayanan, A. Almutairi, *Anal. Chem.* **2011**, *83*, 3943.
- [16] C. Mayer, *Prog. Nucl. Magn. Reson. Spectrosc.* **2002**, *40*, 307.
- [17] K. D. M. Harris, C. E. Hughes, A. Williams, G. R. Edwards-Gau, *Acta Crystallogr. Sect. C* **2017**, *73*, 137.
- [18] A. E. Raymond, R. R. Edward, P. K. John, *Philos. Trans. R. Soc. London Ser. A* **1981**, *299*, 505.

- [19] T. Polenova, R. Gupta, A. Goldbourt, *Anal. Chem.* **2015**, *87*, 5458.
- [20] B. Reif, S. E. Ashbrook, L. Emsley, M. Hong, *Nat. Rev. Methods Primers* **2021**, *1*, 1.
- [21] C. Lucas-Torres, A. Wong, *Metabolites* **2019**, *9*, 29.
- [22] J. E. Jenkins, M. R. Hibbs, T. M. Alam, *ACS Macro Lett.* **2012**, *1*, 910.
- [23] W. E. Maas, F. H. Laukien, D. G. Cory, *J. Am. Chem. Soc.* **1996**, *118*, 13085.
- [24] T. M. Alam, J. E. Jenkins, in *Advanced Aspects of Spectroscopy* (Ed: M. A. Farrukh), IntechOpen, p. 279.
- [25] K. Westesen, H. Bunjes, M. H. J. Koch, *J. Controlled Release* **1997**, *48*, 223.
- [26] C. Mayer, in *Annual Reports on NMR Spectroscopy* (Ed: G. A. Webb), **2005**, pp. 205–258.
- [27] C. Mayer, D. Hoffmann, M. Wohlgemuth, *Int. J. Pharm.* **2002**, *242*, 37.
- [28] T. Kojima, M. Karashima, K. Yamamoto, Y. Ikeda, *Mol. Pharmaceutics* **2018**, *15*, 3901.
- [29] C. E. Hughes, K. D. M. Harris, *J. Phys. Chem. A* **2008**, *112*, 6808.
- [30] C. E. Hughes, P. A. Williams, K. D. M. Harris, *Angew. Chem. Int. Ed.* **2014**, *53*, 8939.
- [31] C. L. Jones, C. E. Hughes, H. H.-M. Yeung, A. Paul, K. D. M. Harris, T. L. Easun, *Chem. Sci.* **2021**, *12*, 1486.
- [32] P. Horcajada, T. Chalati, C. Serre, B. Gillet, C. Sebrie, T. Baati, J. F. Eubank, D. Heurtaux, P. Clayette, C. Kreuz, J.-S. Chang, Y. K. Hwang, V. Marsaud, P.-N. Bories, L. Cynober, S. Gil, G. Férey, P. Couvreur, R. Gref, *Nat. Mater.* **2010**, *9*, 172.
- [33] J. Yang, Y.-W. Yang, *Small* **2020**, *16*, 1906846.
- [34] M. D. L. Vuong, Y. Horbenko, M. Fregnaud, I. Christodoulou, C. Martineau-Corcos, P. Levitz, A.-L. Rollet, R. Gref, M. Haouas, *ACS Appl. Mater. Interfaces* **2024**, *16*, 2086.
- [35] M. D. L. Vuong, I. Christodoulou, M. Porcino, S. Dong, B. Lassalle-Kaiser, M. Haouas, R. Gref, C. Martineau-Corcos, *Chem. Mater.* **2022**, *34*, 8178.
- [36] G. M. Bernard, A. Goyal, M. Miskolzie, R. McKay, Q. Wu, R. E. Wasylshen, V. K. Michaelis, *J. Magn. Reson.* **2017**, *283*, 14.
- [37] C. Martineau, F. Decker, F. Engelke, F. Taulelle, *Solid State Nucl. Magn. Reson.* **2013**, *55–56*, 48.
- [38] Y. Lian, H. Jiang, J. Feng, X. Wang, X. Hou, P. Deng, *Talanta* **2016**, *150*, 485.
- [39] M. Haouas, F. Taulelle, C. Martineau, *Prog. Nucl. Magn. Reson. Spectrosc.* **2016**, *94–95*, 11.
- [40] T. Kiss, I. Sovago, R. B. Martin, *Inorg. Chem.* **1991**, *30*, 2130.
- [41] V. Agostoni, P. Horcajada, V. Rodriguez-Ruiz, H. Willaime, P. Couvreur, C. Serre, R. Gref, *Green Mater.* **2013**, *1*, 209.
- [42] A. G. Marquez, A. Demessence, A. E. Platero-Prats, D. Heurtaux, P. Horcajada, C. Serre, J.-S. Chang, G. Férey, V. Antonio de la Pena-O'Shea, C. Boissiere, D. Grosso, C. Sanchez, *Eur. J. Inorg. Chem.* **2012**, 5165.

Manuscript received: January 7, 2024  
Revised manuscript received: March 26, 2024  
Accepted manuscript online: March 31, 2024  
Version of record online: April 23, 2024